Research Square

Preprints are preliminary reports that have not undergone peer review.
They should not be considered conclusive, used to inform clinical practice,
or referenced by the media as validated information.

IMU-Based and Auto-Tuned Virtual Decomposition Control for a Hydraulic Rock-Breaker Boom

Mehdi Heydari Shahna

mehdi.heydarishahna@tuni.fi

Tampere University

Pauli Mustalahti

Tampere University

Jouni Mattila

Tampere University

Research Article

Keywords:

Posted Date: November 18th, 2026

DOI: https://doi.org/10.21203/rs.3.rs-11737527/v1

License: This work is licensed under a Creative Commons Attribution 4.0 International License.
Read Full License

Additional Declarations: The authors declare no competing interests.

IMU-Based and Auto-Tuned Virtual Decomposition Control for a Hydraulic Rock-Breaker Boom

Mehdi Heydari Shahna, Pauli Mustalahti, and Jouni Mattila

***Abstract*—Joint encoders of rock-breaker booms sit at exposed pins, where impacts and falling rock damage them. This article controls a hydraulic rock-breaker boom using protected link-mounted inertial measurement units (IMUs) after a one-time calibration. Building on a pairwise complementary filter, each joint observer transports the specific forces of the two adjacent IMUs to the joint point with each link's own gyro rate, so that the joint-angle measurement depends on no estimate. A common Lyapunov function proves the confidence-weighted proportional–integral observer input-to-state stable for arbitrary weight trajectories above a floor, within an explicit error region, and because control errors do not enter the observer, observers and virtual decomposition control (VDC) form a cascade: the boom-joint loops are proved regionally input-to-state stable with the pressure-compensated valves modeled as velocity sources with delays, gain mismatch and dead zones, including online tuning. An auto-tuning procedure identifies each valve's joint assignment, flow gains, dead zones and loop delay through the feedback in use and sets the position gains to satisfy the stability condition. On a 10-t Rambooms X88-540-R boom, the observer deviated from the encoders by 0.07–0.11° RMS, and with IMU-only feedback the boom joints tracked a strike-cycle sequence within 0.12–0.21° RMS.**

***Index Terms*—Hydraulic manipulator, inertial measurement unit (IMU), input-to-state stability (ISS), state observer.**

I. Introduction

SECONDARY rock breaking at grizzlies and ore passes keeps the material flowing in mines and quarries: oversize boulders are reduced by a hydraulic breaker on a pedestal boom. The booms are mostly operated manually or remotely [1], and research on their automation has concentrated on perception, strike-pose selection and learned breaking policies [2]–[4]. Autonomous breaking also needs closed-loop motion control with feedback sensors that survive shock, vibration, dust, falling rock and kilojoule-class blows [5]: joint encoders sit at the exposed pins with their cables along the links, draw-wire cylinder sensors can be hit by debris [6], and contact-type joint sensors are generally impractical there [7].

MEMS inertial measurement units (IMUs), in contrast, can be bolted to protected link surfaces and read at 1 kHz over real-time fieldbuses. Joint-angle sensing with accelerometers and gyros is surveyed in [8]. Accelerometers served as joint-angle sensors of a mini-excavator [7]. IMUs also complement cylinder-stroke sensors of excavators [6] and measure their swing angle [9]. For heavy-duty hydraulic manipulators, Vihonen *et al.* developed geometry-aided estimators [10]–[13]: the forward-kinematic model [12] estimates every IMU's attitude after subtracting rigid-body accelerations propagated from the base, and the joint-space model [13] forms a gravity-referenced joint-angle reference from the IMUs of two adjacent links and fuses it with their relative gyro rate in a proportional–integral (PI) complementary filter whose correction is attenuated by a confidence weight. MEMS-based state feedback and virtual decomposition control (VDC) were demonstrated on a laboratory crane [14], [15]. VDC [16], [17] decomposes a robot into rigid links and actuators, designs a local controller for each subsystem and guarantees stability of the whole nonlinear system through virtual power flows (VPFs) at the subsystem boundaries. It has given stability-guaranteed, high-precision motion, force and impedance control of heavy-duty hydraulic manipulators and cranes [18], [19], and its modularity is shared by recent robust designs [5], [20]; see [21] for a survey. It needs accurate joint states, and its actuator level depends on valve characteristics such as large spool overlaps, direction-dependent flow gains and slow spool actuation [22]. Methods for valve identification, dead-zone compensation and gain tuning address parts of the commissioning (Section IV), but a multi-joint controller on a new machine still needs expert tuning.

This article adopts the pairwise architecture of [13] (adjacent-link IMUs, relative gyro rate, PI complementary filter, confidence-dependent correction) and addresses three open questions. (i) The joint-space reference of [13] needs the joint angle, in practice its estimate, and the effect of this dependence and of the state-dependent weight on stability has not been analyzed. (ii) Observer theory for VDC [23] assumes measured joint positions, so that the stability of a VDC fed by estimated joint angles, and of the velocity-level VDC of valve-controlled machines without pressure feedback, is open. (iii) To the best of the authors' knowledge, closed-loop control of a full-scale breaker boom from link IMUs, with a self-commissioning controller, has not been reported. The contributions are as follows. 1) *Joint-point transport* (Section III): the specific force of each IMU is transported to the joint point with its own link's gyro rate, so that the joint-angle measurement depends on no estimate; it differs from the joint-space reference of [13] by one term, derived here, which makes the measurement depend on the estimation error, so that the effective observer gain varies with the boom accelerations. 2) *Stability analysis* (Sections III and V): a common Lyapunov function proves the confidence-weighted PI filter input-to-state stable (ISS) for arbitrary weight trajectories above a floor, a

The authors are with the Faculty of Engineering and Natural Sciences, Tampere University, 33720 Tampere, Finland. Corresponding author: Mehdi Heydari Shahna, Korkeakoulunkatu 7, 33720 Tampere, Finland (telephone: +358405920406; e-mail: mehdi.heydarishahna@tuni.fi).

The complete proofs, the controller code, the analysis scripts and a video of the experiments with the synchronized digital twin are available at https://github.com/Mehdi-Heydari-Shahna/rambooms-imu-vdc.

new analysis of an existing filter. Because control errors do not enter the observer, observers and VDC form a cascade, which is regionally ISS for the boom joints under the velocity-level VDC of the machine, with velocity-source actuators with distributed delays, gain mismatch, dead zones and online tuning, and for the full VDC of the digital twin. 3) *Auto-tuned velocity-level VDC* (Section IV): commissioning without prior knowledge of the valves, not even their wiring, in which the actuators are identified through the feedback that will close the loop and the position gains satisfy the stability condition with a margin. 4) *Experiments, digital twin and ablation* (Sections VI–VIII): closed-loop control of a 10-t Rambooms X88-540-R boom through a strike-cycle sequence on IMU feedback alone; a CAD-based MuJoCo digital twin [24], aligned with the machine and synchronized with the logged experiments, which the supplementary video shows side by side with the machine; and an ablation on identical sensor data (real logs and the digital twin with hammer impacts) that isolates the lever-arm terms, confidence weighting, weight floor and gain selection and compares with the filters of [12], [13].

II. System Description and Problem Statement

The test system (Fig. 1) is a Rambooms X88-540-R pedestal boom of about 10 t with a 270° swing range and a reach of 7 m. The *slew* joint rotates the turret about the vertical pedestal axis; the *lift* joint raises the lift link (pin distance $L_1 = 2.75\,\mathrm{m}$) with two parallel cylinders, the *tilt* joint rotates the dipper ($L_2 = 3.5\,\mathrm{m}$) and the *crowd* joint the tool link, formed by an adapter and the breaker whose chisel tip lies $L_3 = 3.40\,\mathrm{m}$ from the crowd pin, each with one cylinder. With the joint angles $\boldsymbol{q} = [q_1, q_2, q_3]^\top$ (lift, tilt, crowd), the absolute link angles $\phi_k = \sum_{j\le k} q_j$ in the vertical boom plane and the slew angle ψ, the chisel-tip position follows from $(\psi, \boldsymbol{q})$, the pin distances and the chisel offset by planar forward kinematics. Each cylinder spans one joint through a three-bar linkage, with the length $L_{c,i}(q_i)$ and the moment arm $m_i(q_i) = \partial L_{c,i}/\partial q_i$ from the CAD. Each joint is driven by one section of a Sauer-Danfoss PVG 120 pressure-compensated, load-sensing proportional valve, as used in commercial rock-breaker systems (Fig. 2a; the lift cylinders share one). While $p_{LS} + p_0 \le p_S$ (p_{LS}: load pressure, p_S: supply pressure), its compensator keeps the pressure drop across the metering edge near the spring preload p_0, so that the piston velocity follows the spool opening nearly independently of the load [22]. The spool overlap causes large dead zones (29% and 31% of the command range for the last link of a boom of this type), and the spool actuation is slow (250 ms for a full opening) [22]. Each actuator thus acts as a velocity source with direction-dependent gains, dead zones and a delay (Fig. 2b).

Each of the three boom links carries an EtherCAT IMU based on a Murata SCHA63T-K03, with ±300°/s gyros and $\pm 6\,g$ accelerometers [25]. IMU k is mounted with its z axis approximately along the joint axes, at the in-plane lever arm $\boldsymbol{r}_k = [s_k, n_k]^\top$ from the proximal joint, with an unknown in-plane mounting angle β_k. Its in-plane axes are rotated by $\theta_k = \phi_k + \beta_k$, so that, with the planar rotation $\mathbf{R}(\theta)$, its accelerometer and z gyro read

$$\boldsymbol{f}_k = \mathbf{R}(\theta_k)^\top(\boldsymbol{a}_k - \boldsymbol{g}) + \boldsymbol{b}_{a,k} + \boldsymbol{n}_{a,k}, \tag{1}$$

$$\omega_{z,k} = \sigma_k\dot{\phi}_k + \boldsymbol{\kappa}_k^\top\boldsymbol{\omega}_{xy,k} + b_{g,k} + n_{g,k}, \tag{2}$$

where $\boldsymbol{a}_k$ is the in-plane acceleration of the sensor point, $\boldsymbol{g} = [0, -g_0]^\top$, $\boldsymbol{b}_{a,k}$ and $b_{g,k}$ are biases, σ_k is the gyro scale factor and $\boldsymbol{\kappa}_k$ couples the out-of-plane rates $\boldsymbol{\omega}_{xy,k}$ (nonzero during slewing) into the z channel; $\boldsymbol{\omega}_k = [\boldsymbol{\omega}_{xy,k}^\top, \omega_{z,k}]^\top$. At rest, $\angle\boldsymbol{f}_k := \operatorname{atan2}(f_{x,k}, f_{y,k})$ returns θ_k; in operation, $\boldsymbol{a}_k$ contains link, slew and base accelerations and, during blows, impact transients and structural ringing. Absolute joint encoders (SIKO WV58MR, 14-bit resolution per encoder revolution) serve only as the reference for the one-time IMU calibration, for commissioning and for evaluation.

After a one-time calibration against joint-angle references, estimate the boom-joint angles and rates from the IMU signals $\{\boldsymbol{f}_k, \boldsymbol{\omega}_k\}_{k=1}^3$ alone at 1 kHz, and control the boom along a strike-cycle sequence (approach, vertical descent and press, hold, retraction) with a VDC whose actuator parameters are identified automatically on the machine, with a stability guarantee for the observer-based closed loop. Gravity carries no information about the slew angle ψ; the boom IMUs supply its rate, and its angle comes from an absolute slew sensor or, in the IMU-only experiment, from the gyro rates (Section VII).

III. Pairwise Inertial Joint Observer

The parameters $(s_k, n_k, \beta_k, \boldsymbol{b}_{a,k})$ are identified once by robust nonlinear least squares of (1), with the rigid-body acceleration computed from reference joint angles (here, the encoders) and the gyro rates of a calibration run that includes slewing; $(\sigma_k, \boldsymbol{\kappa}_k, b_{g,k})$ of (2) follow from linear least squares. The calibrated rate of IMU k and the relative rate of joint i are

$$\tilde{\omega}_{z,k} = \big(\omega_{z,k} - \boldsymbol{\kappa}_k^\top\boldsymbol{\omega}_{xy,k} - b_{g,k}\big)/\sigma_k, \qquad \tilde{\omega}_i = \tilde{\omega}_{z,i} - \tilde{\omega}_{z,i-1}, \tag{3}$$

with $\tilde{\omega}_{z,0} = 0$; the remaining biases are estimated online.

Let J be a point of link k with link coordinates $\boldsymbol{r}_J$ (proximal joint: $\boldsymbol{r}_J = \mathbf{0}$; distal joint: $\boldsymbol{r}_J = [L_k, 0]^\top$), and $\boldsymbol{\rho}_k = \boldsymbol{r}_k - \boldsymbol{r}_J$ (Fig. 3). For a rigid link, $\boldsymbol{a}_k = \boldsymbol{a}_J + \mathbf{R}(\phi_k)(\ddot{\phi}_k\boldsymbol{\rho}_k^\perp - \dot{\phi}_k^2\boldsymbol{\rho}_k)$ with $[x, y]^\perp = [-y, x]$. Inserting this into (1) and using $\mathbf{R}(\theta_k)^\top\mathbf{R}(\phi_k) = \mathbf{R}(\beta_k)^\top$ gives the specific force of the joint point in the axes of IMU k,

$$\boldsymbol{f}_{J|k} = \tilde{\boldsymbol{f}}_k - \boldsymbol{c}_k \approx \mathbf{R}(\theta_k)^\top(\boldsymbol{a}_J - \boldsymbol{g}), \tag{4}$$

with the lever-arm term $\boldsymbol{c}_k := \mathbf{R}(\beta_k)^\top(\bar{\alpha}_k\boldsymbol{\rho}_k^\perp - \bar{\omega}_k^2\boldsymbol{\rho}_k)$, where $\tilde{\boldsymbol{f}}_k := \bar{\boldsymbol{f}}_k - \boldsymbol{b}_{a,k}$, $\bar{\boldsymbol{f}}_k$ and $\bar{\omega}_k$ are the specific force and $\tilde{\omega}_{z,k}$ after a common 20-Hz second-order low-pass filter, and $\bar{\alpha}_k = \frac{d}{dt}\bar{\omega}_k$. Identical filtering keeps the phases consistent, and differentiating the filtered rate avoids the noise amplification of raw differences [10], [11]. Only the link's own gyro is needed, and no acceleration is propagated from the base [12], so that errors do not accumulate along the chain. For joint i, IMU i is transported to its proximal and IMU $i-1$ to its distal joint; for $i = 1$, the parent is the level turret with $\boldsymbol{f}_{J|0} = [0, g_0]^\top$.

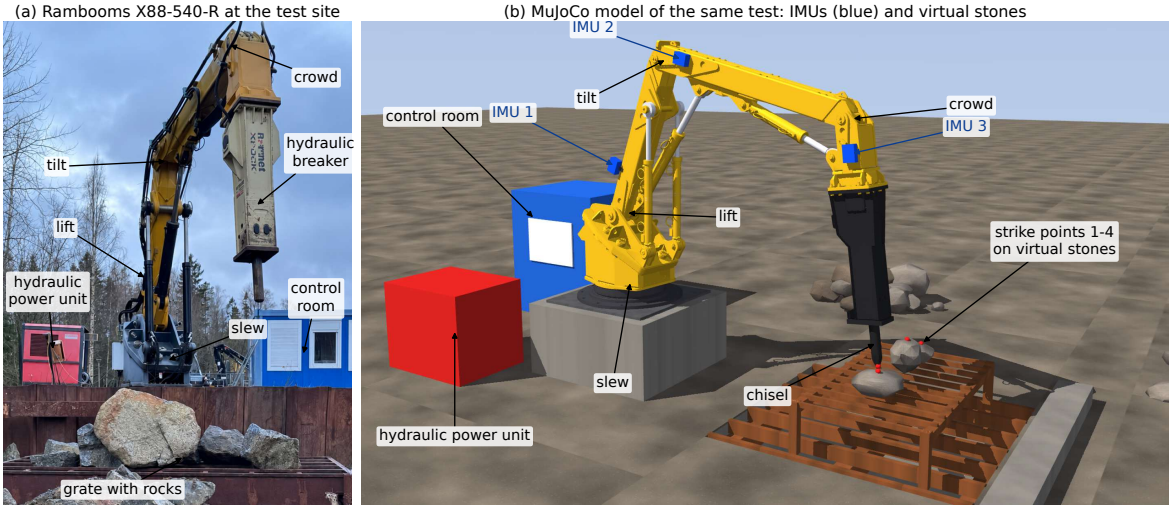


Fig. 1. Test system. (a) Rambooms X88-540-R boom at the test site with the hydraulic power unit (red) and the control room (blue). (b) MuJoCo model from the manufacturer's CAD: link IMUs (enlarged, blue), the boom at the first press point of run I and virtual stones at the four strike points.

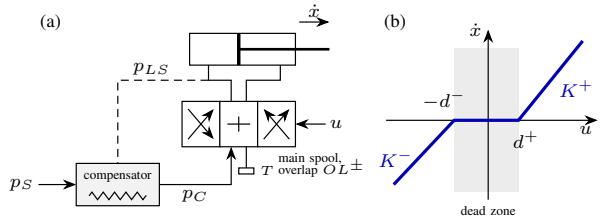


Fig. 2. Valve-controlled actuator of each joint. (a) Pressure-compensated, load-sensing proportional valve (Sauer-Danfoss PVG 120, simplified after [22]); the compensator makes the piston velocity follow the spool opening nearly independently of the load. (b) Resulting velocity characteristic with direction-dependent gains $K^{\pm}$ and dead zones $d^{\pm}$ (spool overlap), identified by Algorithm 1.

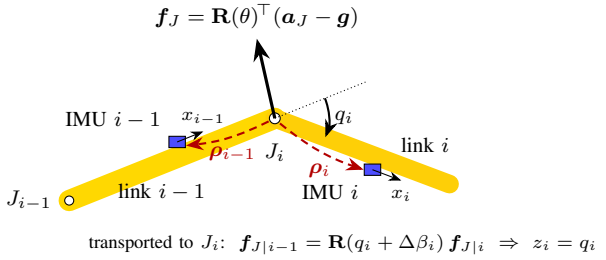


Fig. 3. Pairwise joint-point measurement: both IMUs transport their specific force to the joint J_i (lever arms $\boldsymbol{\rho}$) with their own gyro rates; the angle between the transported vectors differs from q_i by the constant $\Delta\beta_i$, whatever the motion of J_i.

Proposition 1 (Invariance). *With* $\Delta\beta_i = \beta_i - \beta_{i-1}$, *exact transported vectors satisfy* $\boldsymbol{f}_{J|i-1} = \mathbf{R}(q_i + \Delta\beta_i)\boldsymbol{f}_{J|i}$ *and, for* $q_i \in (-\pi, \pi]$,

$$z_i := \operatorname{wrap}\left(\angle \boldsymbol{f}_{J|i} - \angle \boldsymbol{f}_{J|i-1} - \Delta\beta_i\right) = q_i \tag{5}$$

whenever the in-plane component of $\boldsymbol{a}_J - \boldsymbol{g}$ *is nonzero.*

Proof. Both vectors equal $\mathbf{R}(\theta_{(\cdot)})^\top(\boldsymbol{a}_J - \boldsymbol{g})$, and $\angle(\mathbf{R}(\vartheta)^\top \boldsymbol{v}) = \angle \boldsymbol{v} + \vartheta$, so that the angles differ by $\theta_i - \theta_{i-1} = q_i + \Delta\beta_i$. ∎

For joints 2 and 3, the gravity direction, the acceleration of the joint point (caused by the proximal links, the slew or the base) and the inclination of the boom plane cancel; joint 1 assumes a level, stationary pedestal. During slewing, the in-plane centripetal acceleration (up to 2° of error in z_3 at 0.34 rad/s) is removed by adding $\bar{\boldsymbol{\omega}}_{xy,k}(\bar{\boldsymbol{\omega}}_{xy,k}^\top \boldsymbol{\rho}'_k) - \|\bar{\boldsymbol{\omega}}_{xy,k}\|^2 \boldsymbol{\rho}'_k$, $\boldsymbol{\rho}'_k = \mathbf{R}(\beta_k)^\top \boldsymbol{\rho}_k$, to $\boldsymbol{c}_k$. Impacts and ringing, seen differently by the two sensors, remain; they are detected by the in-plane vector residual

$$r_i = \left\|\mathbf{R}(\hat{q}_i + \Delta\beta_i)\boldsymbol{f}_{J|i} - \boldsymbol{f}_{J|i-1}\right\| \tag{6}$$

at the estimate $\hat{q}_i$; out-of-plane components are excluded because they differ between sensors whose z axes are tilted (by about 5° here) even at rest.

The joint-space model of [13] relates the two sensors of joint i through the acceleration of the child sensor point relative to the parent sensor point, which, by (4), is $\boldsymbol{c}_i - \mathbf{R}(q_i + \Delta\beta_i)^\top \boldsymbol{c}_{i-1}$ in the child axes; the reference is the angle between the parent specific force and the child specific force minus this term. Rotating the parent's lever-arm term into the child axes requires the joint angle, which, in practice and in the implementation compared in Section VIII, is the current estimate:

$$z_i^{\mathrm{js}} := \operatorname{wrap}\left(\angle\left(\tilde{\boldsymbol{f}}_i - \boldsymbol{c}_i + \mathbf{R}(\hat{q}_i + \Delta\beta_i)^\top \boldsymbol{c}_{i-1}\right) - \angle \tilde{\boldsymbol{f}}_{i-1} - \Delta\beta_i\right). \tag{7}$$

Both (5) and (7) use the same signals and lever arms; they differ only in where $\boldsymbol{c}_{i-1}$ is applied.

Proposition 2 (Estimate dependence). *For exact signals and* $e_{q,i} := \hat{q}_i - q_i$, *define the circular measurement error* $\Delta z_i := \operatorname{wrap}(z_i^{\mathrm{js}} - q_i)$. *Then* $|\Delta z_i| \le \arcsin(|e_{q,i}|\|\boldsymbol{c}_{i-1}\|/\|\tilde{\boldsymbol{f}}_{i-1}\|)$ *if the argument is defined and below one, and* $\Delta z_i = \varkappa_i e_{q,i} + O(e_{q,i}^2)$ *as* $e_{q,i} \to 0$, *with* $\varkappa_i := \tilde{\boldsymbol{f}}_{i-1}^\top \boldsymbol{c}_{i-1}/\|\tilde{\boldsymbol{f}}_{i-1}\|^2$; *in contrast,* $\operatorname{wrap}(z_i - q_i) = 0$ *for every* $\hat{q}_i$.

Proof. By Proposition 1, $\tilde{\boldsymbol{f}}_i - \boldsymbol{c}_i = \mathbf{R}(q_i + \Delta\beta_i)^\top(\tilde{\boldsymbol{f}}_{i-1} - \boldsymbol{c}_{i-1})$, so that the first vector in (7), rotated by $\mathbf{R}(q_i + \Delta\beta_i)$, is $\tilde{\boldsymbol{f}}_{i-1} + \boldsymbol{d}$ with $\boldsymbol{d} = (\mathbf{R}(-e_{q,i}) - \mathbf{I})\boldsymbol{c}_{i-1}$, $\|\boldsymbol{d}\| \le |e_{q,i}|\|\boldsymbol{c}_{i-1}\|$

and $\boldsymbol{d} = -e_{q,i}\boldsymbol{c}_{i-1}^{\perp} + O(e_{q,i}^2)$. The circular angle change caused by adding $\boldsymbol{d}$ to $\boldsymbol{f}$ is bounded by $\arcsin(\|\boldsymbol{d}\|/\|\boldsymbol{f}\|)$ and locally equals $(f_y d_x - f_x d_y)/\|\boldsymbol{f}\|^2 + O(\|\boldsymbol{d}\|^2)$. ■

With (7), the innovation of the observer below becomes $\varepsilon = v - (1-\varkappa_i)e_{q,i}$ to first order: the weight w is effectively replaced by $w(1-\varkappa_i)$, which depends, through $\boldsymbol{c}_{i-1}$, on the rate and acceleration of link $i-1$, i.e., on the motion generated by the controller. Lemma 1 then requires $w_{\min}(1-\bar{\varkappa}) > k_I/k_P^2$, $\bar{\varkappa} \geq \varkappa_i$, i.e., $\bar{\varkappa} < 0.22$ for the gains used here (roughly $\|\boldsymbol{c}_{i-1}\| < 0.22 g_0$), and for $\varkappa_i > 1$ the correction has the wrong sign. With (5), $\varkappa_i \equiv 0$: the observer error dynamics contain neither an estimate nor a control error, which makes observers and controller a cascade (Section V). The transport removes rigid-body acceleration dependence from the ideal measurement; impact and ringing residuals remain disturbances subject to the bounds and regional conditions of Theorem 1. Section VIII evaluates the remaining differences from the laboratory implementation of [13] (residual, filtering, calibration, weight law and gains).

For every joint (index dropped), the observer fuses the relative rate with the joint-point measurement:

$$\begin{gathered}\tfrac{d}{dt}\hat{q} = \tilde{\omega} - \hat{b} + k_P\, w\, \varepsilon, \qquad \tfrac{d}{dt}\hat{b} = -k_I\, w\, \varepsilon, \qquad \hat{\dot{q}} = \tilde{\omega} - \hat{b}, \\ \varepsilon = \operatorname{wrap}(z - \hat{q}), \qquad w = \max\left\{w_{\min}, \exp(-r^2/c^2)\right\}.\end{gathered} \tag{8}$$

With $w \equiv 1$, (8) is the classical PI complementary filter [13], [26]; w is a redescending Welsch M-estimator weight [27] on (6). For $\tilde{\omega} = \dot{q} + b + n_\omega$, $\dot{b} = \eta$, $z = q + v$ with white noises of intensities N_ω, N_b, N_v, the steady-state Kalman–Bucy filter [28] is (8) with $w \equiv 1$, $k_I = \sqrt{N_b/N_v}$ and $k_P = \sqrt{N_\omega/N_v + 2k_I}$, whose error polynomial $s^2 + k_P s + k_I$ has a damping ratio of at least $1/\sqrt{2}$. Unless otherwise stated in the ablations, the nominal design values are $k_P = 0.8\,\mathrm{s}^{-1}$ and $k_I = k_P^2/64 = 0.01\,\mathrm{s}^{-2}$, the Kalman–Bucy gains for the effective intensity ratios $N_\omega/N_v = 0.62\,\mathrm{s}^{-2}$ and $N_b/N_v = 10^{-4}\,\mathrm{s}^{-4}$ (damping ratio 4), $c = 0.5\,\mathrm{m/s}^2$ and $w_{\min} = 0.02$.

With $v := z - q$, $n_\omega := \tilde{\omega} - \dot{q} - b$, $\eta := \dot{b}$ and $\tilde{\boldsymbol{x}} = [\hat{q} - q,\ \hat{b} - b]^\top$, (8) gives, wherever the wrap is inactive ($|z - \hat{q}| < \pi$),

$$\dot{\tilde{\boldsymbol{x}}} = \underbrace{\begin{bmatrix} -k_P w & -1 \\ k_I w & 0 \end{bmatrix}}_{\mathbf{A}(w)} \tilde{\boldsymbol{x}} + \boldsymbol{\xi}, \qquad \boldsymbol{\xi} = \begin{bmatrix} k_P \\ -k_I \end{bmatrix} w\, v + \begin{bmatrix} n_\omega \\ -\eta \end{bmatrix}. \tag{9}$$

Since w depends on the state and the disturbances, stability of $\mathbf{A}(w)$ for every frozen w does not imply stability.

Lemma 1 (Common Lyapunov function)**.** *Let* $\mathbf{P} = \begin{bmatrix} 1 & k_P/(2k_I) \\ k_P/(2k_I) & k_P^2/(2k_I^2) \end{bmatrix} \succ \mathbf{0}$. *Then* $\mathbf{A}(w)^\top\mathbf{P} + \mathbf{P}\mathbf{A}(w) = -\mathbf{Q}(w)$ *with* $\mathbf{Q}(w) = \begin{bmatrix} k_P w & 1 \\ 1 & k_P/k_I \end{bmatrix}$, *and* $\mathbf{Q}(w) \succ \mathbf{0}$ *if and only if* $w > k_I/k_P^2$. *Hence, if* $w_{\min} > k_I/k_P^2$, $\mathcal{V} = \tilde{\boldsymbol{x}}^\top\mathbf{P}\tilde{\boldsymbol{x}}$ *satisfies* $\dot{\mathcal{V}} \leq -2\mu\mathcal{V}$ *along* $\dot{\tilde{\boldsymbol{x}}} = \mathbf{A}(w(t))\tilde{\boldsymbol{x}}$ *for every weight trajectory* $w(t) \in [w_{\min}, 1]$, *which may be discontinuous and depend on the state and the disturbances, with* $\mu = \frac{1}{2}\lambda_{\min}\big(\mathbf{P}^{-1/2}\mathbf{Q}(w_{\min})\mathbf{P}^{-1/2}\big)$.

Proof. The off-diagonal entries of $\mathbf{A}^\top\mathbf{P} + \mathbf{P}\mathbf{A}$ do not depend on w because $p_{22} = p_{12}k_P/k_I$, and $\det\mathbf{Q}(w) = k_P^2 w/k_I - 1$. Since $\mathbf{Q}(w) - \mathbf{Q}(w_{\min}) = \operatorname{diag}(k_P(w - w_{\min}), 0) \succeq \mathbf{0}$, $\mathbf{Q}(w) \succeq \mathbf{Q}(w_{\min}) \succeq 2\mu\mathbf{P}$ on the whole interval, without gridding w, and $\dot{\mathcal{V}} = -\tilde{\boldsymbol{x}}^\top\mathbf{Q}(w(t))\tilde{\boldsymbol{x}} \leq -2\mu\mathcal{V}$ at every instant. ■

Theorem 1 (ISS of the weighted observer)**.** *Let* $w_{\min} > k_I/k_P^2$, *let* $|v| \leq \bar{v}$, $|n_\omega| \leq \bar{n}$ *and* $|\eta| \leq \bar{\eta}$ *be piecewise continuous, and let* $w(t) \in [w_{\min}, 1]$ *be any piecewise continuous weight trajectory.*
(a) For $\boldsymbol{\xi} \equiv \mathbf{0}$, *the error model* (9) *is globally uniformly exponentially stable, and, in general, with* $\|\boldsymbol{x}\|_\mathbf{P} := (\boldsymbol{x}^\top\mathbf{P}\boldsymbol{x})^{1/2}$,

$$\|\tilde{\boldsymbol{x}}(t)\|_\mathbf{P} \leq e^{-\mu t}\|\tilde{\boldsymbol{x}}(0)\|_\mathbf{P} + \tfrac{1-e^{-\mu t}}{\mu} \sup_{0\leq t'\leq t} \|\boldsymbol{\xi}(t')\|_\mathbf{P}. \tag{10}$$

(b) There are peak gains $\gamma_v, \gamma_n, \gamma_\eta$, *valid for every weight trajectory, such that*

$$|\tilde{x}_1(t)| \leq \sqrt{2}e^{-\mu t}\|\tilde{\boldsymbol{x}}(0)\|_\mathbf{P} + \gamma_v\bar{v} + \gamma_n\bar{n} + \gamma_\eta\bar{\eta} \leq \bar{e}, \tag{11}$$

where $\bar{e} := \sqrt{2}\|\tilde{\boldsymbol{x}}(0)\|_\mathbf{P} + \gamma_v\bar{v} + \gamma_n\bar{n} + \gamma_\eta\bar{\eta}$.
(c) If $\bar{v} + \bar{e} < \pi$, *the wrap stays inactive for all* $t \geq 0$, *and (a) and (b) hold for the observer* (8).

Theorem 1 follows from Lemma 1 with the comparison lemma [29] and invariant-ellipsoid certificates of the peak gains [30]; the complete proof, with the certificates, is given in the supplementary material. For the design values, $k_I/k_P^2 = 1/64 < w_{\min}$, and the eigenvalues $2(k_P w - k_I/k_P)$ and $2k_I/k_P$ of $\mathbf{P}^{-1}\mathbf{Q}(w)$ give $\mu = k_P(w_{\min} - k_I/k_P^2) = 0.0035\,\mathrm{s}^{-1}$ ($1/\mu \approx 5\,\mathrm{min}$), a robustness bound set by the margin of the floor, while the peak gains below quantify the accuracy; for $w = 1$, the fast angle-correction mode has a time constant of approximately 1.3 s, while the slow mode associated with bias estimation has a time constant of approximately 79 s. $\mathbf{P}$ is also a common Lyapunov function of the forward-Euler discretization with the step $h_s = 1\,\mathrm{ms}$, since $(\mathbf{I} + h_s\mathbf{A}(w))^\top\mathbf{P}(\mathbf{I} + h_s\mathbf{A}(w)) - \mathbf{P}$ is matrix-convex in w and negative definite at both vertices. The result is global for (9) and regional for (8), whose only nonlinearities, the weight and the wrap, are covered exactly; no linearization is involved. The certified peak gains $\gamma_v \leq 7.54$, $\gamma_n \leq 168\,\mathrm{s}$ and $\gamma_\eta \leq 7.2 \times 10^3\,\mathrm{s}^2$ give the region of (c), e.g., $\bar{v} < 20°$ for $\bar{n} = \bar{\eta} = 0$ and small initial errors, instead of 0.79° through (10) alone. The theorem holds for any weighting rule with values in $[w_{\min}, 1]$; the Welsch weight also limits the correction by a single sample to a rate of $k_P\pi c/(2\sqrt{2\mathrm{e}}g_0) \approx 0.027\,\mathrm{rad/s}$ unless the sample is off by more than 98° (since $r \geq 2f_\mathrm{m}|\varepsilon|/\pi$, $f_\mathrm{m} \approx g_0$). The floor prevents unbounded gyro drift when samples are rejected for long, and freezing the lever-arm terms while the breaker fires keeps the admitted samples consistent in sustained hammering (Section VIII).

The controller receives $\hat{q}_i$ and the bias-corrected gyro rates $\hat{\dot{q}}_i = \tilde{\omega}_i - \hat{b}_i$, low-passed with a 20-ms time constant, not the derivative of $\hat{q}_i$, which differs by $k_P w\varepsilon$ and contains link accelerations through v: for an inclination measured at the distance ℓ from the joint without transport, $\frac{d}{dt}\hat{q}$ contains $-k_P w(\ell\sin\vartheta_g/g_0)\ddot{q}$ (ϑ_g: angle between tangent and gravity), so that a velocity feedback with gain k_v per unit link inertia scales the apparent inertia by $1 - k_v k_P w\ell\sin\vartheta_g/g_0$, which turns negative for high observer gains. In $\hat{\dot{q}}_i$, accelerometer

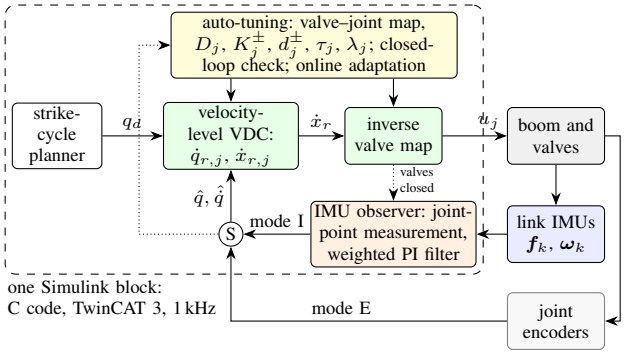


Fig. 4. Control system on the machine: the same auto-tuned velocity-level VDC runs with the encoders (mode E; observer in shadow mode) or with the IMU observer (mode I; encoders only logged). The required wrenches and forces (13) are only monitored; force tracking (full VDC) is used in the digital twin.

information enters only through the bias estimate, with a frequency response from v to $\tilde{x}_2$ of at most $k_I/k_P = 0.0125\,\mathrm{s}^{-1}$ for every frozen weight.

IMUs in the vertical boom plane supply the slew rate without additional hardware, complementing an absolute slew sensor (Section II). For the IMU-only run of Section VII, the slew angle was dead-reckoned from the rates of IMUs 1 and 2 about the gravity direction, with the gyro biases averaged at rest and the angle held while the slew valve was closed and the boom at rest.

IV. Auto-Tuned Virtual Decomposition Control

The slew is indexed by $j = 0$ and the boom joints by $j = i \in \{1, 2, 3\}$; $\hat{q}_j$ and $\hat{\dot{q}}_j$ are the fed-back angles and rates (encoders or observer, Fig. 4). A valve-controlled joint responds to a command after a delay τ_j (spool actuation, oil compressibility, sensing and filtering), so that the position error is formed with the delayed reference,

$$e_j(t) = q_{d,j}(t - \tau_j) - \hat{q}_j(t), \qquad \dot{q}_{r,j}(t) = \dot{q}_{d,j}(t) + \lambda_j\, e_j(t), \tag{12}$$

where $\dot{q}_{r,j}$ is the required joint velocity of VDC [17] and λ_j the position gain; the feedback acts only on deviations from the expected delayed motion, and the delay, which remains in the loop, limits λ_j. Every planned segment starts from the fed-back position. VDC propagates the required link twists $\boldsymbol{V}_{r,i} = \mathbf{U}_{i-1,i}^{\top}(\hat{q}_i)\boldsymbol{V}_{r,i-1} + [0, 0, \dot{q}_{r,i}]^{\top}$ from the base to the tool, $\mathbf{U}_{i-1,i}$ being the force/velocity transformation between the frames of links $i-1$ and i, and the required wrenches back from the tool [16], [18],

$$\begin{aligned} \boldsymbol{F}^*_{r,i} &= \mathbf{M}_i\dot{\boldsymbol{V}}_{r,i} + \mathbf{C}_i\boldsymbol{V}_{r,i} + \boldsymbol{G}_i(\hat{\phi}_i) + \mathbf{K}_{V,i}(\boldsymbol{V}_{r,i} - \hat{\boldsymbol{V}}_i), \\ \boldsymbol{F}_{r,i} &= \boldsymbol{F}^*_{r,i} + \mathbf{U}_{i,i+1}(\hat{q}_{i+1})\boldsymbol{F}_{r,i+1}, \end{aligned} \tag{13}$$

with the link inertia matrices $\mathbf{M}_i$, Coriolis and centrifugal matrices $\mathbf{C}_i$ and gravity wrenches $\boldsymbol{G}_i$ (from the CAD), $\hat{\boldsymbol{V}}_i$ built from $\hat{\dot{q}}$, $\dot{\boldsymbol{V}}_{r,i}$ formed recursively from $\hat{\dot{q}}$ and $\ddot{q}_{r,j} = \ddot{q}_{d,j} + \lambda_j(\dot{q}_{d,j}(t - \tau_j) - \hat{\dot{q}}_j)$, i.e., without differentiating $\hat{q}$, and $\mathbf{K}_{V,i} = 2\mathbf{M}_i\,\mathrm{s}^{-1}$. They give the required cylinder forces $f_{r,i} = [0, 0, 1]\boldsymbol{F}_{r,i}/m_i(\hat{q}_i)$, and the actuators receive the required piston velocities $\dot{x}_{r,i} = m_i(\hat{q}_i)\dot{q}_{r,i}$ (slew: $\dot{x}_{r,0} = \dot{q}_{r,0}$).

Algorithm 1 Automatic tuning of one valve channel

1: With all valves closed for 1 s, record the drift and velocity noise of every joint.
2: Ramp the command at $0.05\,\mathrm{s}^{-1}$; assign the channel to the first joint j whose displacement and velocity exceed noise-scaled thresholds for 30 ms, set D_j from the direction of motion and record the breakaway command u_b.
3: Continue at $0.15\,\mathrm{s}^{-1}$ until 3° of travel or 2°/s, close the valve and wait until all joints rest; repeat steps 2–3 with negative commands.
4: Per direction, fit $|\dot{q}| = K(|u(t - 0.1\,\mathrm{s})| - d)$ to the moving samples (20-ms records) by least squares; if $d < u_b/2$ (slow inertial response, stick–slip), raise d to $u_b - 0.08$ and refit K.
5: Apply a smooth command step (rise time 0.5 s; slew: 1 s) for the nominal joint speed, at most 0.1 above the command of step 3, toward the larger joint-limit margin and back (at most 6° and 60% of the margin); record 5-ms samples.
6: Fit $\dot{q} = K\,\mathcal{L}_T[\max(u(t - \tau) - d, 0)]$ ($\mathcal{L}_T$: first-order lag) by a grid search over $\tau \in [0, 0.4]\,\mathrm{s}$ and $T \in [0, 0.3]\,\mathrm{s}$ with least-squares K; set $\tau_j = \tau + T - \tau_v$ (τ_v: delay of the rate filter, 45 ms for encoder and 25 ms for gyro rates), limited to $[0.03, 0.5]\,\mathrm{s}$; refine K from the steady step speed; set λ_j by (15) and $K_j^{\pm} = K^{\pm}|m_j(q_j)|$.

Full VDC tracks the required cylinder forces using chamber-pressure feedback; actuator VPFs cancel, yielding whole-system stability [17], [18]. This runs in the digital twin. On the machine, the identified valve map realizes the required piston velocities without pressure feedback, while required forces are monitored. This *velocity-level VDC* is decentralized joint-velocity control enabled by pressure compensation. Since actuator VPFs do not cancel, Section V proves stability directly using velocity-source actuators. The steady piston speed is modeled by $|\dot{x}| = K_j^{\pm}(|u| - d_j^{\pm})$ for $|u| > d_j^{\pm}$ (Fig. 2b), with positive direction-dependent gains $K_j^{\pm}$ and dead zones $d_j^{\pm}$, and the valve command is the regularized inverse map

$$u_j = D_j\big(\varsigma_j\, d_j^{\varsigma_j}\min\{|\dot{q}_{r,j}|/v_b,\, 1\} + \dot{x}_{r,j}/K_j^{\varsigma_j}\big), \tag{14}$$

where $D_j \in \{-1, 1\}$ is the valve direction, which absorbs the sign of m_j (taken positive in (14) and Algorithm 1), $\varsigma_j = \operatorname{sgn}\dot{q}_{r,j}$ (during planned motions, $\operatorname{sgn}\dot{q}_{d,j}$) selects the parameters of the direction, and the blend with $v_b = 0.3$°/s removes the discontinuity at rest. A joint at rest without a planned motion is held (valve closed) below an error of 0.12° and released above 0.35°, which prevents limit cycles across the dead zones; commands are limited to $|u_j| \le 0.8$ and to a rate of $5\,\mathrm{s}^{-1}$.

If the valve flow responds fast compared with λ_j, each joint is an integrator with the delay τ_j, and the loop of (12) has the transfer function $\lambda_j e^{-\tau_j s}/s$, with crossover frequency λ_j, phase margin $\pi/2 - \lambda_j\tau_j$ and gain margin $\pi/(2\lambda_j\tau_j)$. The position gain is

$$\lambda_j = \min\{\max\{1/(3\tau_j),\, \lambda_{\mathrm{lo}}\},\, \lambda_{\mathrm{hi}}\}, \tag{15}$$

i.e., a phase margin of 71° and a gain margin of 4.7, with $\lambda_{\mathrm{lo}} = 0.7$ and $\lambda_{\mathrm{hi}} = 2.5\,\mathrm{s}^{-1}$ (at λ_{lo}, at least 62° and 3.3 for delays up to 0.675 s, the largest that the grid of Algorithm 1 represents). Section V gives the nonlinear counterpart of this linear argument.

Algorithm 1 is executed for the valve channels 4, 3, 2, 1 in turn; each channel is assigned to the joint that responds, so that an unexpected wiring is detected. Every test is bounded in command, travel and speed and ends when another joint

moves, and the planner limits the joint speeds to 70% of the identified capacity. A closed-loop check follows: every joint moves out by about 4° at half speed and back; an overshoot beyond $\max\{0.3^\circ, 0.1\times\text{amplitude}\}$ or three sign changes of the error during settling reduce λ_j by 30%, but not below λ_{lo}, and the check is repeated (at most twice). The procedure combines flow-map identification [31], [32], dead-zone compensation [22], [33] and delay-based tuning [34]. It also identifies the valve-to-joint assignment and directions, uses the feedback that will close the loop, and estimates the delay and velocity gain required by (23). Equation (15) gives $\lambda_j\tau_j \le 0.35$, tolerating a combined delay–gain factor of at least 2.85 for the identified pure-delay model; the closed-loop check tests the resulting tuning on the machine.

Online adaptation: (i) While a joint moves steadily, the valve gain of the active direction is adapted by $\dot{K}_j^{\pm} = a_K K_j^{\pm}\big(\hat{\dot{q}}_j/\dot{q}_{r,j}(t-\tau_j-\tau_v)-1\big)$, $a_K = 0.3\,\mathrm{s}^{-1}$, within $[0.6, 1.6]$ times the identified value. (ii) In slow motions, the dead zone of the active direction grows when the joint lags behind the delayed reference and shrinks when it leads, within bounds around the identified value. (iii) Six sign changes of the low-passed error within 5 s indicate an oscillation, e.g., an unmodeled resonance, and reduce λ_j by 30%, but not below λ_{lo}. The delays are not adapted. The task speed starts at half the nominal speed and increases by 0.15 after every strike cycle whose largest error stayed below 1°.

V. Stability of the Observer-Based Closed Loop

Unlike the measured-angle design of [23], this controller uses estimated joint angles. Equation (9) contains no control error, and bounded motion-dependent sensor errors yield an observer–controller cascade. The loop closes at $t = 0$, after Algorithm 1; complete stability proofs are provided in the supplementary material. With the errors $e_{q,j} := \hat{q}_j - q_j$ and $e_{\omega,i} := \hat{\dot{q}}_i - \dot{q}_i$ of the fed-back angles and rates ($e_{q,i} = \tilde{x}_{1,i}$, $e_{\omega,i} = -\tilde{x}_{2,i} + n_{\omega,i}$ before the low-pass), the tracking error of the true angle and the error seen by the controller in (12) are

$$\tilde{e}_j(t) := q_{d,j}(t-\tau_j) - q_j(t), \qquad e_j = \tilde{e}_j - e_{q,j}. \tag{16}$$

Assumption 1 (Sensors)**.** *For every boom joint, v_i, $n_{\omega,i}$ and η_i in* (9) *are piecewise continuous with $|v_i| \le \bar{v}_i$, $|n_{\omega,i}| \le \bar{n}_i$, $|\eta_i| \le \bar{\eta}_i$ and $\bar{v}_i + \bar{e}_i < \pi$, $\bar{e}_i$ being the bound* (11)*; the slew-rate error $\dot{e}_{q,0}$ is piecewise continuous and bounded.*

The bounds include the motion-dependent errors (lever-arm, scale-factor and misalignment residuals, filter lags), which are bounded because valve capacities and actuator forces limit the boom's rates and accelerations.

Assumption 2 (Velocity-source actuators)**.** *On the machine, for $t \ge 0$ and while the commands stay below their limits, every actuator realizes*

$$\dot{q}_j(t) = \int_{[0,h_j]} \zeta_j(t,s)\,\dot{q}_{r,j}(t-s)\,\mathcal{K}_{j,t}(ds) + \delta_j(t), \tag{17}$$

where the probability measure $\mathcal{K}_{j,t}$ on $[0, h_j]$ distributes the command-to-motion delay, $\zeta_j(t,s) \in [\zeta_{\mathrm{lo}}, \zeta_{\mathrm{hi}}]$, $0 < \zeta_{\mathrm{lo}} \le 1 \le \zeta_{\mathrm{hi}}$, is the ratio of the realized to the assumed velocity gain, and $|\delta_j| \le \bar{\delta}_j$; ζ_j, $\mathcal{K}_{j,t}$ and δ_j are piecewise continuous in t with right limits, and ζ_j is measurable in s.

The pressure-compensated valves (Section II) make (17) a physical model: $\mathcal{K}_{j,t}$ contains the spool and pressure dynamics and the sampling, ζ_j the mismatch of the adapted gains, their residual load dependence and the moment-arm ratio $m_j(\hat{q}_j(t-s))/m_j(q_j(t))$, and δ_j the dead-zone mismatch, the blend in (14), leakage and the hold logic. No form of time variation is assumed, so that the online adaptation is covered; a latency of the fed-back angle enlarges h_j.

Assumption 3 (Full VDC)**.** *In the twin: (a) the links are planar rigid bodies, $\mathbf{M}_i\dot{\boldsymbol{V}}_i + \mathbf{C}_i(\omega_i)\boldsymbol{V}_i + \boldsymbol{G}_i(\phi_i) = \boldsymbol{F}_i^* + \boldsymbol{F}_{\mathrm{d},i}$, with bounded disturbance wrenches $\boldsymbol{F}_{\mathrm{d},i}$; (b) every cylinder obeys $\dot{f}_i = \mathcal{B}(u_{f,i} - c_{p,i}(x_i)\dot{x}_i)$, the valve flow is inverted exactly with the measured pressures, and the actuator controller of [18] is $u_{f,i} = \dot{f}_{r,i}/\mathcal{B} + c_{p,i}(\hat{x}_i)\hat{\dot{x}}_i + k_{f,i}(f_{r,i} - f_i) + k_{x,i}(\dot{x}_{r,i} - \hat{\dot{x}}_i)$, $k_{f,i}, k_{x,i} > 0$, with $\hat{x}_i = L_{c,i}(\hat{q}_i)$, $\hat{\dot{x}}_i = m_i(\hat{q}_i)\hat{\dot{q}}_i$ and bounded $\dot{f}_{r,i}$; (c) $\dot{\boldsymbol{V}}_{r,i}$ is formed as in Section IV; (d) $\mathcal{S}$ is a compact set of states on which the joints are within their ranges, $m_i \ne 0$ between q_i and $\hat{q}_i$, the valves are unsaturated and $|e_{q,i}| \le \pi/2$.*

Lemma 2 (Error injection)**.** *Let $\dot{q}_{r,j}^{\circ} := \dot{q}_{d,j} + \lambda_j\tilde{e}_j$, let $\boldsymbol{V}_{r,i}^{\circ}$ be the required twists computed from $\dot{q}_r^{\circ}$ with the true angles, and let $\Delta\boldsymbol{V}_i := \boldsymbol{V}_{r,i}^{\circ} - \boldsymbol{V}_i$, $\Delta\dot{q}_i := \dot{q}_{r,i}^{\circ} - \dot{q}_i$, $\Delta f_i := f_{r,i} - f_i$, $\dot{x}_{r,i}^{\circ} := m_i(q_i)\dot{q}_{r,i}^{\circ}$, and $p_i := \Delta\boldsymbol{V}_i^{\top}(\boldsymbol{F}_{r,i} - \boldsymbol{F}_i)$ the VPF at joint i, $\boldsymbol{F}_i$ being the wrench of link $i-1$ on link i (p_4: tool tip). Then:*
(a) $\dot{q}_{r,j} = \dot{q}_{r,j}^{\circ} - \lambda_j e_{q,j}$;
(b) under Assumption 2, for $t \ge h_j$,

$$\dot{\tilde{e}}_j(t) = -\int a_j(t,s)\big[\tilde{e}_j(t-s) - e_{q,j}(t-s)\big]\mathcal{K}_{j,t}(ds) + \varpi_j(t), \tag{18}$$

with $a_j(t,s) := \zeta_j(t,s)\lambda_j(t-s)$ and $\varpi_j(t) := \dot{q}_{d,j}(t-\tau_j) - \int \zeta_j(t,s)\dot{q}_{d,j}(t-s)\mathcal{K}_{j,t}(ds) - \delta_j(t)$;
(c) under Assumption 3 with constant gains $\lambda_i > 0$, $\nu_i := \frac{1}{2}\Delta\boldsymbol{V}_i^{\top}\mathbf{M}_i\Delta\boldsymbol{V}_i$ and $\nu_{\mathrm{a},i} := \Delta f_i^2/(2\mathcal{B}k_{x,i})$ satisfy

$$\begin{aligned}\textstyle\sum_{i=1}^{3}(\dot{\nu}_i + \dot{\nu}_{\mathrm{a},i}) = &-\textstyle\sum_{i=1}^{3}\big(\Delta\boldsymbol{V}_i^{\top}\mathbf{K}_{V,i}\Delta\boldsymbol{V}_i + \frac{k_{f,i}}{k_{x,i}}\Delta f_i^2\big)\\ &-\textstyle\sum_{i=1}^{3}\Delta\boldsymbol{V}_i^{\top}\boldsymbol{F}_{\mathrm{d},i} - p_4 + \varrho,\end{aligned} \tag{19}$$

where the VPF mismatch caused by the estimates is

$$\begin{aligned}\varrho = &\textstyle\sum_{i=1}^{3}\big[\Delta\dot{q}_i(m_i(\hat{q}_i) - m_i(q_i))f_{r,i} + \Delta f_i\Delta_{\mathrm{a},i} - \Delta\boldsymbol{V}_i^{\top}\boldsymbol{\Delta}_i\big]\\ &-\textstyle\sum_{i=1}^{2}\Delta\boldsymbol{V}_i^{\top}\big[\mathbf{U}_{i,i+1}(\hat{q}_{i+1}) - \mathbf{U}_{i,i+1}(q_{i+1})\big]\boldsymbol{F}_{r,i+1},\end{aligned} \tag{20}$$

$\boldsymbol{\Delta}_i$ and $\Delta_{\mathrm{a},i}$ being the changes of $\boldsymbol{F}_{r,i}^*$ and of the actuator law caused by the estimates. On $\mathcal{S}$, $|\varrho| \le b_\varrho\|\boldsymbol{\chi}\|(\|\boldsymbol{e}_q\| + \|\boldsymbol{e}_\omega\|)$ for some $b_\varrho > 0$, $\boldsymbol{\chi} := [\Delta\boldsymbol{V}_1^{\top}, \Delta\boldsymbol{V}_2^{\top}, \Delta\boldsymbol{V}_3^{\top}, \Delta f_1, \Delta f_2, \Delta f_3]^{\top}$.

With exact estimates, $\varrho = 0$, and (19) is the VPF cancellation of the VDC theorem [17], [18]; the angle errors enter through $-\lambda_j e_{q,j}$, m_i, $\mathbf{U}_{i,i+1}$ and $\boldsymbol{G}_i$, the rate errors through $\mathbf{K}_{V,i}(\boldsymbol{V}_{r,i} - \hat{\boldsymbol{V}}_i)$, $\dot{\boldsymbol{V}}_{r,i}$ and $\hat{\dot{x}}_i$. On the machine, only (a) and (b) matter.

Lemma 3 (Delay loop)**.** *Let $\mathcal{K}_t$ be probability measures on $[0, h]$ and $a(t,s) \in [a_{\mathrm{lo}}, a_{\mathrm{hi}}]$, $0 < a_{\mathrm{lo}} \le a_{\mathrm{hi}}$, with $\mathcal{K}_t$, a and u piecewise continuous in t with right limits and a measurable*

in s, and let y, bounded on $[t_0-2h, t_0-h]$ and absolutely continuous afterwards, satisfy

$$\dot{y}(t) = -\int_{[0,h]} a(t,s)\, y(t-s)\, \mathcal{K}_t(ds) + u(t), \qquad t \geq t_0 - h. \tag{21}$$

If $\vartheta := a_{\mathrm{hi}} h < 1$, then, for $t \geq t_0$, with $\Gamma := (1+\vartheta)/(a_{\mathrm{lo}}(1-\vartheta))$ and $\mu_{\mathrm{d}} > 0$ solving $\mu_{\mathrm{d}} = a_{\mathrm{lo}}(1 - \vartheta e^{2\mu_{\mathrm{d}} h})$,

$$|y(t)| \leq e^{-\mu_{\mathrm{d}}(t-t_0)} \|y\|_{[t_0-2h,t_0]} + 2\Gamma \|u\|_{[t_0-h,t]}, \tag{22}$$

and $\limsup |y| \leq \Gamma \limsup |u|$.

The condition $a_{\mathrm{hi}} h < 1$ holds however a and $\mathcal{K}_t$ vary. For a constant gain and a pure delay, the exact limit is $ah < \pi/2$, on which the phase margin of (15) rests, and under arbitrary variations, stability extends to $a_{\mathrm{hi}} h < 3/2$ [35]; the bound 1 is the price of the explicit ISS estimate of the Razumikhin-type argument [36]. Lemma S1 of the supplementary material extends the result to kernels with a small tail beyond h.

Theorem 2 (Velocity-level VDC with the observers)**.** *Let Assumptions 1 and 2 hold, $w_{\min} > k_I/k_P^2$, $\lambda_j(t) \in [\lambda_{\mathrm{lo}}, \bar{\lambda}_j]$, $\bar{\lambda}_j$ being the value set by* (15)*, and*

$$\vartheta_j := \zeta_{\mathrm{hi}} \bar{\lambda}_j h_j < 1, \qquad j = 0, \ldots, 3, \tag{23}$$

and let μ_j, Γ_j be the constants μ_{d}, Γ of Lemma 3 for $a_{\mathrm{lo}} = \zeta_{\mathrm{lo}} \lambda_{\mathrm{lo}}$, $a_{\mathrm{hi}} = \zeta_{\mathrm{hi}} \bar{\lambda}_j$ and $h = h_j$. Then, while the commands stay below their limits:
(i) the observer errors satisfy (11)*, independently of the controller;*
(ii) for $t \geq 2h_j$, with $\limsup |\tilde{e}_j| \leq \Gamma_j(\zeta_{\mathrm{hi}} \bar{\lambda}_j \limsup |e_{q,j}| + \limsup |\varpi_j|)$,

$$|\tilde{e}_j(t)| \leq e^{-\mu_j(t-2h_j)} \|\tilde{e}_j\|_{[0,2h_j]} + 2\Gamma_j \big(\zeta_{\mathrm{hi}} \bar{\lambda}_j \|e_{q,j}\|_{[0,t]} + \|\varpi_j\|_{[h_j,t]}\big); \tag{24}$$

(iii) for each boom joint, there are $k_1, k_2 > 0$ such that, with $\bar{\mu}_j := \frac{1}{2}\min\{\mu_j, \mu\}$ and $t \geq 2h_j$,

$$|\tilde{e}_j(t)| \leq k_1 e^{-\bar{\mu}_j t} \big(\|\tilde{e}_j\|_{[0,2h_j]} + \|\tilde{\boldsymbol{x}}_j(0)\|_{\mathbf{P}}\big) + k_2 \big(\bar{v}_j + \bar{n}_j + \bar{\eta}_j + \|\varpi_j\|_{[h_j,t]}\big), \tag{25}$$

i.e., observers, velocity-level VDC and actuators form an ISS cascade, and with ideal sensors and $\varpi_j \equiv 0$ (e.g., set-point regulation with $\delta_j \equiv 0$), $(\tilde{e}_j, \tilde{\boldsymbol{x}}_j) \to \mathbf{0}$ exponentially;
(iv) the slew error $\tilde{e}_0$ satisfies (ii), with $e_{q,0}$ the error of the fed-back slew angle, i.e., that of an absolute slew sensor or, for the dead-reckoned angle, the accumulated drift $e_{q,0}(t) = e_{q,0}(0) + \int_0^t \dot{e}_{q,0}$.

Equation (25) requires no coupling condition between observer and controller gains; its constants and decay rate are worst-case bounds. For the identified pure-delay model, $h_j = \tau_j$ and $\zeta_j \equiv 1$, the margin $1/(\bar{\lambda}_j \tau_j)$ is at least 2.85 for all joints and both runs (Table I), leaving at least 1.4 for doubled valve gains. For the fitted delay-plus-lag model, supplementary Lemma S1 holds for lag shares T/τ_j up to 0.45/0.66 (boom/slew), or 0.29/0.39 when $\zeta_j \in [0.8, 1.2]$.

Theorem 3 (Full VDC with the observers)**.** *Let Assumptions 1 and 3 hold, $w_{\min} > k_I/k_P^2$, $\mathbf{K}_{V,i} \succ \mathbf{0}$ and $\lambda_i > 0$ constant. Let $e_{f,i}$ be $-\tilde{x}_{2,i} + n_{\omega,i}$ low-passed like the fed-back rate (time constant T_v), $d_{f,i} := e_{\omega,i} - e_{f,i}$ the low-pass lag of the true rate, $T_v \dot{d}_{f,i} = -d_{f,i} - T_v \ddot{q}_i$, and let $\boldsymbol{d}_{\mathrm{c}}$ collect $\boldsymbol{F}_{\mathrm{d},i}$, the tool-tip wrench, $\dot{q}_{d,i}(t-\tau_i) - \dot{q}_{d,i}(t)$ and $\ddot{q}_{d,i}$. There are $T_v^*, k_e, \alpha_W, \gamma_W > 0$, depending on $\mathcal{S}$, such that, for $T_v \leq T_v^*$ and along trajectories in $\mathcal{S}$,*

$$W_{\mathrm{c}} := \tfrac{k_e}{2}\|\tilde{\boldsymbol{e}}\|^2 + \textstyle\sum_{i=1}^{3}(\nu_i + \nu_{\mathrm{a},i} + \frac{1}{2} d_{f,i}^2) \tag{26}$$

satisfies

$$\dot{W}_{\mathrm{c}} \leq -\alpha_W W_{\mathrm{c}} + \gamma_W \big(\|\boldsymbol{e}_q\|^2 + \|\boldsymbol{e}_f\|^2 + \|\boldsymbol{d}_{\mathrm{c}}\|^2\big), \tag{27}$$

where $\boldsymbol{e}_q$ and $\boldsymbol{e}_f$ are bounded independently of the controller (Theorem 1). Hence, observers and full VDC form an ISS cascade from $(\boldsymbol{\xi}_i, n_{\omega,i}, \boldsymbol{d}_{\mathrm{c}})$ to $(\tilde{\boldsymbol{e}}, \boldsymbol{\chi}, \boldsymbol{d}_f, \tilde{\boldsymbol{x}}_i)$ while the trajectory stays in $\mathcal{S}$, which holds if a sublevel set of W_{c} that contains the resulting bound lies, with the observer bounds, in $\mathcal{S}$; with ideal sensors and $\boldsymbol{d}_{\mathrm{c}} \equiv \mathbf{0}$, all errors converge to zero exponentially.

Remark 1 (Coupling and scope)**.** *For the composite function $W_{\mathrm{c}} + c_{\mathrm{o}} V_{\mathrm{o}}$, with an observer function V_{o} of the observer errors $\tilde{\boldsymbol{x}}_{\mathrm{e}} = (\tilde{\boldsymbol{x}}_i, e_{f,i})$ and the control errors $\boldsymbol{v} = (\tilde{\boldsymbol{e}}, \boldsymbol{\chi}, \boldsymbol{d}_f)$, the proofs give, up to disturbance terms, $\dot{W}_{\mathrm{c}} \leq -\alpha_1\|\boldsymbol{v}\|^2 + \gamma_{\mathrm{c}}\|\boldsymbol{v}\|\|\tilde{\boldsymbol{x}}_{\mathrm{e}}\|$ and $\dot{V}_{\mathrm{o}} \leq -\alpha_2\|\tilde{\boldsymbol{x}}_{\mathrm{e}}\|^2 + \gamma_{\mathrm{o}}\|\tilde{\boldsymbol{x}}_{\mathrm{e}}\|\|\boldsymbol{v}\|$ with $\gamma_{\mathrm{o}} = 0$, so that the coupling condition $4\alpha_1 c_{\mathrm{o}} \alpha_2 > (\gamma_{\mathrm{c}} + c_{\mathrm{o}}\gamma_{\mathrm{o}})^2$ holds for large c_{o} and restricts no gain; with $\gamma_{\mathrm{o}} > 0$, it would require the small-gain condition $\alpha_1\alpha_2 > \gamma_{\mathrm{c}}\gamma_{\mathrm{o}}$. The joint-space measurement* (7)*, whose error $\varkappa_i e_{q,i}$ grows with the link accelerations, introduces such a coupling, as does a fed-back rate that contains accelerometer signals. Both theorems hold on explicit regions (inactive wrap, unsaturated commands, states in $\mathcal{S}$), and the oscillation detector of the online adaptation complements them for lightly damped hydraulic modes.*

VI. Implementation and Experimental Setup

The observer, the auto-tuning, the VDC, the task planner and the mode logic form one MATLAB Function block in Simulink, whose C code, generated with Simulink Coder and the TwinCAT target for MATLAB/Simulink, runs as a TwinCAT 3 module in a 1-ms task on a Beckhoff industrial PC that reads the three IMUs over EtherCAT and the four joint encoders over a 500 kbit/s CAN bus, and transmits the four valve commands over a separate 250 kbit/s CAN bus. The mode input closes all valves (0), runs the task with encoder feedback and the observer in shadow mode (1, run E), or runs the same task with the observer outputs, without using the encoder inputs (2, run I); a mode change starts a new run with auto-tuning, so that nothing identified with one feedback source is reused with the other. The block outputs and all sensor signals were logged at 1 kHz. The observer used the design values of Section III and a calibration identified on a log with slewing recorded 18 days earlier. An operator supervised the tests and could stop the boom at any time. Both runs started at rest near the home pose and executed, without operator input, the auto-tuning of all valves, the closed-loop check and the strike-cycle sequence, which visits four strike points at reaches of 4.85–4.95 m and slew angles of $-10°$ to $+10°$ from the start, with the breaker axis inclined by $82°$ below the horizontal (Fig. 1b). Each strike cycle (Fig. 5a) consists of

TABLE I
ACTUATOR PARAMETERS IDENTIFIED BY THE AUTO-TUNING (RUN E: ENCODER FEEDBACK; RUN I: IMU-ONLY FEEDBACK)

joint (valve, D)	run	τ [ms]	λ [s^{-1}]	d^+	d^-	K^+	K^-
slew (1, +)	E	395	0.70*	0.23	0.39	6.8 (10.0)	13.0 (11.7)
	I	500	0.70	0.24	0.31	6.4 (9.5)	9.2 (11.1)
lift (2, +)	E	185	1.80	0.33	0.29	70 (93)	183 (187)
	I	160	2.08	0.34	0.30	69 (83)	206 (194)
tilt (3, −)	E	150	2.22	0.27	0.33	73 (116)	115 (183)
	I	145	2.30	0.34	0.30	85 (117)	230 (205)
crowd (4, −)	E	160	2.08	0.31	0.27	213 (128)	213 (151)
	I	135	2.47	0.31	0.31	206 (124)	249 (165)

Gains per unit command: slew in °/s, cylinders in mm/s; dead zones in units of the command range; in parentheses: adapted gains at the end of the run. *From (15): 0.84, reduced to λ_{lo} by the closed-loop check.

a joint-space move with slewing to an approach pose 0.55 m above the stone top (quintic profiles; peak joint speeds of up to 2.7/1.5/1.9/3.5°/s for slew/lift/tilt/crowd), a vertical straight-line descent of the chisel tip at 0.15 m/s to 0.10 m above the top, pressing at 0.05 m/s to 0.06 m below the top, a 3-s hold and a retraction to 0.70 m above the top, all speeds scaled by the speed factor. The four strike points were visited twice, i.e., eight strike cycles per run, without rocks and without firing the breaker. Run I (IMU-only feedback, slew angle dead-reckoned) was executed first and run E later.

VII. EXPERIMENTAL RESULTS

In both runs, auto-tuning mapped valve channels 1–4 to slew/lift/tilt/crowd with identical directions (Table I). Delays were 135–185 ms for the boom joints, consistent with slow spool actuation (Section II), and reached the 500-ms identification limit for the least-damped slew axis. Equation (15) initially gave boom gains of 1.8–2.5 s^{-1} and slew gains of 0.84/0.70 s^{-1} (runs E/I); run E's check reduced the slew gain to λ_{lo}, lowering overshoot from $0.46°$ to $0.17°$ (limit $0.41°$). After subtracting τ_v, encoder-based delays remained 25/5/25 ms longer for lift/tilt/crowd, consistent with feedback latency. Dead zones spanned 0.23–0.39 (crowd: 0.27–0.31, close to [22]), with larger lift dead zones against gravity and up to threefold directional gain differences. Initial gains differed up to twofold between feedback sources and poses; adaptation brought agreement within 13%, although four of 16 reached bounds: both run E tilt gains at 1.6 and both positive crowd gains at 0.6 times their identified values.

Observer-to-encoder RMS deviations for lift/tilt/crowd were 0.09/0.08/0.11° in run E and 0.08/0.07/0.10° in run I (Table II, Fig. 5b), showing comparable accuracy in shadow and feedback operation, consistent with the cascade structure (Section V). Static calibration offsets dominated: run I's resting deviations were 0.08/0.05/0.12°, and crowd offsets at press poses were $0.15°$–$0.16°$. Strike-cycle maxima were 0.23/0.26/0.30°; transients up to $0.71°$ occurred only during abrupt slew-valve step tests. Weights fell below 0.5 in less than 0.02% of strike-cycle samples and 1–5% of tuning samples. Encoder latency of 10–40 ms changed RMS deviations by less than $0.003°$.

Both runs completed eight strike cycles without intervention, reaching full speed from the fifth. Boom-joint tracking

TABLE II
RESULTS OF THE MACHINE EXPERIMENTS

errors in deg	run	slew	lift	tilt	crowd
observer error, RMS	E	0.03	0.09	0.08	0.11
	I	0.23	0.08	0.07	0.10
observer error, max	E	0.20	0.55	0.71	0.41
	I	0.45	0.44	0.44	0.43
tracking error, RMS	E	0.28	0.08	0.11	0.18
	I	0.48	0.12	0.14	0.21
w.r.t. delayed reference	E	0.19	0.06	0.07	0.09
	I	0.40	0.11	0.11	0.13

	run E	run I
tip tracking error, RMS/max [mm]	27/89	45/126
delayed ref., RMS (lat./in-plane) [mm]	19 (16/10)	37 (34/13)
press-point error, mean±SD [mm]	14±6	36±12
tip estimate error, RMS/max [mm]	11/23	25/41
tuning/check/sequence [s]	116/68/357	125/58/359

RMS was 0.08–0.18° (run E) and 0.12–0.21° (run I) against undelayed references, and 0.06–0.13° against the regulated references delayed by τ_j, with per-cycle standard deviations of 0.01–0.03°. Errors against the controller's own feedback were 0.06/0.07/0.09° and 0.06/0.09/0.10°, respectively, indicating the contribution of estimation error in run I.

The gyro-based slew estimate remained within $0.20°$ of the encoder in run E and drifted by $-0.38°$ in run I (maximum deviation $0.45°$). Drift accumulated during motion: approximately $-0.16°$ in point-to-point moves, $-0.08°$ in descents, $-0.07°$ in tuning/checking and $-0.06°$ in presses/retractions/returns; the angle was held during holds. Slew delays of 395/500 ms produced reference lags of 0.30/0.36° RMS, while tracking errors against delayed references were 0.19/0.40°, including drift (Table II). Tip tracking RMS was 27/45 mm (runs E/I), predominantly lateral, with slew lag alone contributing 25/31 mm at approximately 4.9 m reach. At the press points (Fig. 6), run E stopped 14 ± 6 mm from target; its lateral error (6 ± 12 mm) lay within the slew hold band ($0.35°$, 30 mm). Run I stopped 36 ± 12 mm away, with lateral error 34 ± 13 mm comprising 24 ± 8 mm of drift-dependent slew estimation error and 10 mm of control error; radial error (-9.8 ± 0.8 mm) reflected static calibration offsets. IMU feedback thus achieved approximately 1-cm boom-plane placement at the press poses. An absolute slew reference combined with IMU-derived rate addresses accumulated integration drift (Theorem 2(iv)).

VIII. COMPARISON AND ABLATION

The observers were compared on three 1-kHz boom logs (219, 139 and 106 s), covering single-joint and coordinated motions with 33° and 20° slewing at up to 0.34 rad/s. Parameters calibrated on each of the two slewing logs were applied unchanged to the other two (four train→test pairs), with identical signals for all observers. Baselines comprised laboratory link-wise PI, pairwise [13] and forward-kinematic [12] filters, verified against their earlier results, and a corrected forward-kinematic filter using identified geometry, heading-invariant inclinations and calibration-selected gains. The proposed observer achieved 0.12/0.12/0.18° joint RMS, dominated by static offsets (0.11/0.11/0.18° at rest), and reduced

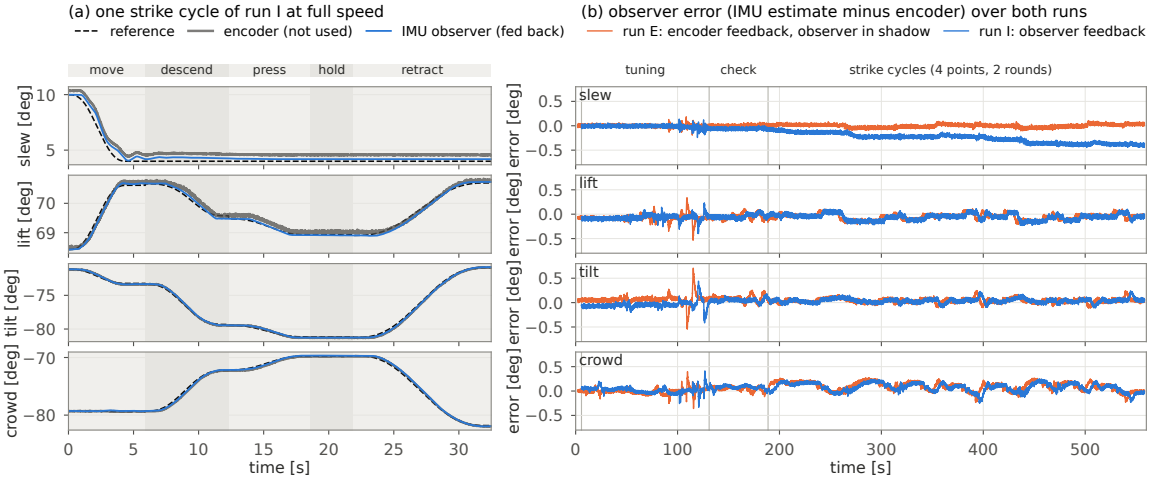


Fig. 5. Machine experiments. (a) One strike cycle of the IMU-only run at full speed: reference, encoder angles (logged, not used) and observer estimates (fed back). (b) Observer error against the encoders over both runs (vertical lines: phases of run I).

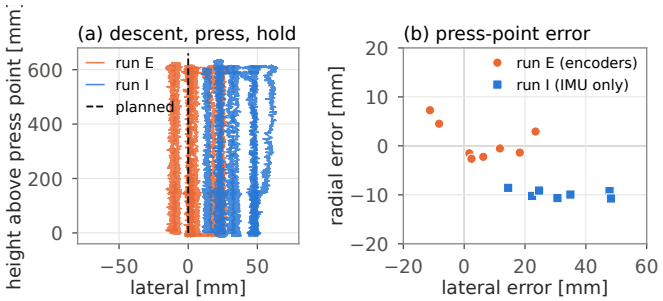


Fig. 6. Chisel tip in the strike cycles, from the encoder angles. (a) Descent, press and hold of all eight cycles relative to the planned press point. (b) Mean tip error over the last 2.5 s of the 3-s holds.

TABLE III
CROSS-VALIDATED JOINT-ANGLE ESTIMATION ON REAL LOGS OF THE BOOM (MEAN OVER FOUR TRAIN→TEST PAIRS; JOINT ERRORS IN DEG, TIP ERRORS IN MM; LAB: LABORATORY IMPLEMENTATION)

	RMS			max (worst pair)			tool tip	
Observer	q_1	q_2	q_3	q_1	q_2	q_3	RMS	max
link-wise filter (lab)	0.17	0.66	0.83	1.37	5.85	7.30	55	471
pairwise filter [13] (lab)	0.22	0.44	0.58	1.62	3.55	3.27	40	316
fwd.-kin. filter [12] (lab)	0.44	0.65	0.47	4.16	5.64	3.23	36	251
fwd.-kin. filter, corrected	**0.09**	0.13	0.20	**0.37**	1.43	**0.90**	18	130
proposed observer	0.12	**0.12**	**0.18**	0.84	**0.77**	1.29	**13**	**54**

tip RMS by factors of 2.8–4.2 relative to laboratory implementations (Table III). The corrected forward-kinematic filter had comparable joint errors (lower for q_1), but 37% larger tip RMS and 2.4 times larger worst tip error under fast slewing. The laboratory pairwise filter's squared-exponential weight on a three-dimensional residual ($k_P = 13.1\,\mathrm{s}^{-1}$) rejected most samples because tilted sensors' out-of-plane forces differed by up to $1.8\,\mathrm{m/s}^2$; errors reached 3.55°. Without weighting, its joint RMS rose to 0.48/0.97/1.16°, with peaks of 23°. The k_P sweeps and calibration-only selection use $k_I = k_P^2/64$ with $w_{\min} = 0.02$; the hand-tuned comparison uses $k_P = 2.5\,\mathrm{s}^{-1}$ and $k_I = 0.025\,\mathrm{s}^{-2}$. The single-element ablations (Table IV) show that weighting barely changes joint RMS but reduces worst tip error from 248 to 54 mm. Norm gating only partly achieves this because it misses vector rotations that preserve magnitude. Across $c \in [0.35, 2]\,\mathrm{m/s}^2$ and $k_P \in [0.5, 0.8]\,\mathrm{s}^{-1}$, tip RMS/max remained 12.9–13.9/54–64 mm. Calibration-only selection (k_P = 0.3–0.5 s^{-1}, c = 2 $\mathrm{m/s}^2$) changed joint RMS by at most 0.01°. Removing lever-arm terms raised tilt/crowd RMS by about 50%/33%. Proposition 2 isolates the difference between (7) and (5); the tables compare complete implementations and ablate lever-arm compensation, weighting, its floor and gains. Impacts were simulated in a CAD-based MuJoCo 3 twin [24], with closed-chain cylinders, orifice/compressibility dynamics [37], SCHA63T-K03-matched

TABLE IV
ABLATION ON IDENTICAL SENSOR DATA (ONE CHANGE PER ROW)

change	real logs	digital twin
none (proposed)	0.12/0.12/0.18°; tip 13/54 mm	0.18/0.52; 640 blows: 1.8
no confidence weight	tip 17/248 mm; joint RMS alike	0.66/2.31; ringing: 5.8; 640 blows: 3.7; in loop: tip after firing 16 → 32 mm
norm gating instead	tip max 94 mm	0.47/1.50; ringing: 4.6
no lever-arm terms ($\boldsymbol{c}_k = \mathbf{0}$)	tilt/crowd RMS ×1.5/×1.3	0.15/0.56; tilt RMS of task 0.21 → 0.34; in loop: tip tracking 31 → 56 mm
no slew-centripetal term	tip max 102 mm	largest error of task 0.83 → 0.95
no weight floor	floor inactive	640 blows: 0.6
lever-arm terms frozen while firing	– (no firing)	640 blows: 0.29
hand-tuned $k_P = 2.5\,\mathrm{s}^{-1}$	tip 14/69 mm	max 0.68
k_P, c selected on cal. logs	0.13/0.12/0.19°; tip 14/72 mm	–
pairwise filter [13]	Table III	0.40/1.56; 640 blows: 6.7
fwd.-kin. filter, corrected	Table III	0.20/0.56; ringing: 0.6; 640 blows: 1.0

Real logs: held out (Table III); joint RMS lift/tilt/crowd. Twin: crowd error RMS/max [deg] while firing, proposed observer in the loop; ringing: max. while firing with up to 3× nominal ringing; 640 blows: max. in a 640-blow burst; in loop: variant fed back.

IMU noise, bias and filters [25] at 1 kHz, and 2.5-kJ, 9-Hz blows with 150-N s recoil and modal ringing. Machine tests involved no firing. The twin reproduced piston positions within 0.52 mm and static crowd-cylinder force with correlation 0.996, and replayed machine logs alongside site video. Across five randomized four-boulder simulations, full VDC with proposed-observer feedback broke all 20 boulders with 31 mm tip RMS (encoders: 28 mm). Alternatives received identical signals; separate feedback runs removed weighting or lever-arm compensation. The pairwise baseline used laboratory gains and identified calibration. During firing, crowd-error maxima were 0.52° (proposed), 2.3° (unweighted), 1.5° (norm gating) and 1.56° (pairwise). The corrected forward-kinematic filter reached 0.56°, with a lower whole-task maximum (0.60° versus 0.83°) but a higher real-log maximum (1.43° versus 1.29°). During 640 blows on a boulder, freezing lever-arm terms while firing limited error to 0.3°; otherwise, rectified gyro ringing and biased samples admitted by the weight floor produced 1.8° error. Feeding back the derivative of a link-wise filter state as the rate made the loop unstable at the start pose.

IX. Discussion and Conclusion

Three protected link IMUs with joint-point transport and automatically commissioned velocity-level VDC controlled a 10-t rock-breaker boom through strike cycles after one-time calibration with slewing. Observer deviations from the encoders were 0.07–0.11° RMS across shadow and IMU-feedback runs, consistent with the cascade analysis. Commissioning took about 3 min; the identified pure-delay model satisfied Theorem 2 with margins of at least 2.85, or 1.4 for doubled valve gains. The analysis establishes regional ISS of the weighted observer for arbitrary weights above the floor and of its cascades with velocity-level and full VDC under the stated assumptions. In the machine-aligned CAD twin, crowd error stayed within 0.52° during firing in five randomized four-boulder simulations. The prolonged 640-blow burst reached 1.8° without freezing lever-arm terms, versus 0.3° with freezing.

Acknowledgment

This work was supported by the Finnish Foundation for Technology Promotion (Tekniikan Edistämissäätiö) through the Post Docs in Companies (PoDoCo) program.

References

[1] E. Duff, C. Caris, A. Bonchis, K. Taylor, C. Gunn, and M. Adcock, "The development of a telerobotic rock breaker," in *Field and Service Robotics* (Springer Tracts in Advanced Robotics). Berlin, Germany: Springer, 2010, pp. 411–420.

[2] S. Lampinen, L. Niu, L. Hulttinen, J. Niemi, and J. Mattila, "Autonomous robotic rock breaking using a real-time 3D visual perception system," *J. Field Robot.*, vol. 38, no. 7, pp. 980–1006, Oct. 2021.

[3] P. Samtani, F. Leiva, and J. Ruiz-del-Solar, "Learning to break rocks with deep reinforcement learning," *IEEE Robot. Autom. Lett.*, vol. 8, no. 2, pp. 1077–1084, Feb. 2023.

[4] F. Leiva, C. Canales, M. Valenzuela, and J. Ruiz-del-Solar, "Data-driven control of hydraulic impact hammers under strict operational and control constraints," arXiv:2601.07813, Jan. 2026.

[5] M. Hejrati and J. Mattila, "Impact-resilient orchestrated robust controller for heavy-duty hydraulic manipulators," *IEEE/ASME Trans. Mechatronics*, vol. 30, no. 6, pp. 5283–5294, Dec. 2025.

[6] D. Sun *et al.*, "Analysis of the position recognition of the bucket tip according to the motion measurement method of excavator boom, stick and bucket," *Sensors*, vol. 20, no. 10, Art. no. 2881, May 2020.

[7] F. Ghassemi, S. Tafazoli, P. D. Lawrence, and K. Hashtrudi-Zaad, "Design and calibration of an integration-free accelerometer-based joint-angle sensor," *IEEE Trans. Instrum. Meas.*, vol. 57, no. 1, pp. 150–159, Jan. 2008.

[8] P. Cheng and B. Oelmann, "Joint-angle measurement using accelerometers and gyroscopes—A survey," *IEEE Trans. Instrum. Meas.*, vol. 59, no. 2, pp. 404–414, Feb. 2010.

[9] S. Kalantar, "IMU based system for vertical axis joint angle estimation for swing boom excavators," U.S. Patent 11 834 813 B2, Dec. 5, 2023.

[10] J. Vihonen, J. Honkakorpi, J. Mattila, and A. Visa, "Geometry-aided angular acceleration sensing of rigid multi-body manipulator using MEMS rate gyros and linear accelerometers," in *Proc. IEEE/RSJ Int. Conf. Intell. Robots Syst. (IROS)*, Nov. 2013, pp. 2514–2520.

[11] J. Vihonen, J. Honkakorpi, J. Mattila, and A. Visa, "Novel pairwise coupled kinematic solution for algebraic angular acceleration estimation of serial link manipulators," in *Proc. IEEE Int. Conf. Robot. Autom. (ICRA)*, May 2015, pp. 809–814.

[12] J. Vihonen, J. Honkakorpi, J. Tuominen, J. Mattila, and A. Visa, "Linear accelerometers and rate gyros for rotary joint angle estimation of heavy-duty mobile manipulators using forward kinematic modeling," *IEEE/ASME Trans. Mechatronics*, vol. 21, no. 3, pp. 1765–1774, Jun. 2016.

[13] J. Vihonen, J. Mattila, and A. Visa, "Joint-space kinematic model for gravity-referenced joint angle estimation of heavy-duty manipulators," *IEEE Trans. Instrum. Meas.*, vol. 66, no. 12, pp. 3280–3288, Dec. 2017.

[14] J. Honkakorpi, J. Vihonen, and J. Mattila, "MEMS-based state feedback control of multi-body hydraulic manipulator," in *Proc. IEEE/RSJ Int. Conf. Intell. Robots Syst. (IROS)*, Nov. 2013, pp. 4419–4425.

[15] J. Koivumäki, J. Honkakorpi, J. Vihonen, and J. Mattila, "Hydraulic manipulator virtual decomposition control with performance analysis using low-cost MEMS sensors," in *Proc. IEEE/ASME Int. Conf. Adv. Intell. Mechatronics (AIM)*, Jul. 2014, pp. 910–917.

[16] W.-H. Zhu, Y.-G. Xi, Z.-J. Zhang, Z. Bien, and J. De Schutter, "Virtual decomposition based control for generalized high dimensional robotic systems with complicated structure," *IEEE Trans. Robot. Autom.*, vol. 13, no. 3, pp. 411–436, Jun. 1997.

[17] W.-H. Zhu, *Virtual Decomposition Control: Toward Hyper Degrees of Freedom Robots* (Springer Tracts in Advanced Robotics, vol. 60). Berlin, Germany: Springer, 2010.

[18] J. Koivumäki and J. Mattila, "Stability-guaranteed force-sensorless contact force/motion control of heavy-duty hydraulic manipulators," *IEEE Trans. Robot.*, vol. 31, no. 4, pp. 918–935, Aug. 2015.

[19] J. Koivumäki and J. Mattila, "Stability-guaranteed impedance control of hydraulic robotic manipulators," *IEEE/ASME Trans. Mechatronics*, vol. 22, no. 2, pp. 601–612, Apr. 2017.

[20] M. Hejrati and J. Mattila, "Orchestrated robust controller for precision control of heavy-duty hydraulic manipulators," *IEEE Trans. Autom. Sci. Eng.*, vol. 22, pp. 14284–14305, 2025.

[21] J. Mattila, J. Koivumäki, D. G. Caldwell, and C. Semini, "A survey on control of hydraulic robotic manipulators with projection to future trends," *IEEE/ASME Trans. Mechatronics*, vol. 22, no. 2, pp. 669–680, Apr. 2017.

[22] S. Lampinen, J. Koivumäki, J. Mattila, and J. Niemi, "Model-based control of a pressure-compensated directional valve with significant dead-zone," in *Proc. ASME/BATH Symp. Fluid Power Motion Control (FPMC)*, Sarasota, FL, USA, Oct. 2019, Paper FPMC2019-1664.

[23] J.-P. Humaloja, J. Koivumäki, L. Paunonen, and J. Mattila, "Decentralized observer design for virtual decomposition control," *IEEE Trans. Autom. Control*, vol. 67, no. 5, pp. 2529–2536, May 2022.

[24] E. Todorov, T. Erez, and Y. Tassa, "MuJoCo: A physics engine for model-based control," in *Proc. IEEE/RSJ Int. Conf. Intell. Robots Syst. (IROS)*, Oct. 2012, pp. 5026–5033.

[25] Murata Electronics Oy, "SCHA63T-K03: 6-DOF XYZ-axis gyroscope and xyz-axis accelerometer with digital SPI interface," Data Sheet, Doc. No. 8019, Rev. 1. Accessed: Oct. 30, 2026. [Online]. Available: https://www.murata.com/en-global/products/sensor/gyro/overview/lineup/scha63t

[26] R. Mahony, T. Hamel, and J.-M. Pflimlin, "Nonlinear complementary filters on the special orthogonal group," *IEEE Trans. Autom. Control*, vol. 53, no. 5, pp. 1203–1218, Jun. 2008.

[27] P. W. Holland and R. E. Welsch, "Robust regression using iteratively reweighted least-squares," *Commun. Statist.—Theory Methods*, vol. 6, no. 9, pp. 813–827, 1977.

[28] R. E. Kalman and R. S. Bucy, "New results in linear filtering and prediction theory," *J. Basic Eng.*, vol. 83, no. 1, pp. 95–108, Mar. 1961.
[29] H. K. Khalil, *Nonlinear Systems*, 3rd ed. Upper Saddle River, NJ, USA: Prentice-Hall, 2002.
[30] J. Abedor, K. Nagpal, and K. Poolla, "A linear matrix inequality approach to peak-to-peak gain minimization," *Int. J. Robust Nonlinear Control*, vol. 6, no. 9–10, pp. 899–927, Nov. 1996.
[31] S. Liu and B. Yao, "Automated onboard modeling of cartridge valve flow mapping," *IEEE/ASME Trans. Mechatronics*, vol. 11, no. 4, pp. 381–388, Aug. 2006.
[32] P. Opdenbosch, N. Sadegh, W. Book, and A. Enes, "Auto-calibration based control for independent metering of hydraulic actuators," in *Proc. IEEE Int. Conf. Robot. Autom. (ICRA)*, May 2011, pp. 153–158.
[33] A. Mohanty and B. Yao, "Integrated direct/indirect adaptive robust control of hydraulic manipulators with valve deadband," *IEEE/ASME Trans. Mechatronics*, vol. 16, no. 4, pp. 707–715, Aug. 2011.
[34] S. Skogestad, "Simple analytic rules for model reduction and PID controller tuning," *J. Process Control*, vol. 13, no. 4, pp. 291–309, Jun. 2003.
[35] J. A. Yorke, "Asymptotic stability for one dimensional differential-delay equations," *J. Differ. Equ.*, vol. 7, pp. 189–202, 1970.
[36] A. R. Teel, "Connections between Razumikhin-type theorems and the ISS nonlinear small gain theorem," *IEEE Trans. Autom. Control*, vol. 43, no. 7, pp. 960–964, Jul. 1998.
[37] H. E. Merritt, *Hydraulic Control Systems*. New York, NY, USA: Wiley, 1967.



Mehdi Heydari Shahna received the D.Sc. (Tech.) degree with distinction in Automation Science and Engineering from Tampere University, Finland, in 2025. He is currently a postdoctoral researcher at Tampere University. His research interests include physical AI, robot learning, safe control, and robust control.



Pauli Mustalahti received the M.Sc. degree from Tampere University of Technology in 2016 and the D.Sc. (Tech.) degree in Automation Science and Engineering from Tampere University in 2023. He is a postdoctoral researcher in the Unit of Automation Technology and Mechanical Engineering, Tampere University, Tampere, Finland. His research interests include nonlinear model-based control of robotic manipulators.



Jouni Mattila received an M.Sc. and Ph.D. in automation engineering from Tampere University of Technology, Tampere, Finland, in 1995 and 2000, respectively. He is currently a professor of machine automation with the Unit of Automation Technology and Mechanical Engineering at Tampere University. His research interests include machine automation, nonlinear-model-based control of robotic manipulators, and energy-efficient control of heavy-duty mobile manipulators.

LIST OF FIGURES

1 Test system. (a) Rambooms X88-540-R boom at the test site with the hydraulic power unit (red) and the control room (blue). (b) MuJoCo model from the manufacturer's CAD: link IMUs (enlarged, blue), the boom at the first press point of run I and virtual stones at the four strike points. 3
2 Valve-controlled actuator of each joint. (a) Pressure-compensated, load-sensing proportional valve (Sauer-Danfoss PVG 120, simplified after [22]); the compensator makes the piston velocity follow the spool opening nearly independently of the load. (b) Resulting velocity characteristic with direction-dependent gains $K^{\pm}$ and dead zones $d^{\pm}$ (spool overlap), identified by Algorithm 1. 3
3 Pairwise joint-point measurement: both IMUs transport their specific force to the joint J_i (lever arms $\boldsymbol{\rho}$) with their own gyro rates; the angle between the transported vectors differs from q_i by the constant $\Delta\beta_i$, whatever the motion of J_i. 3
4 Control system on the machine: the same auto-tuned velocity-level VDC runs with the encoders (mode E; observer in shadow mode) or with the IMU observer (mode I; encoders only logged). The required wrenches and forces (13) are only monitored; force tracking (full VDC) is used in the digital twin. 5
5 Machine experiments. (a) One strike cycle of the IMU-only run at full speed: reference, encoder angles (logged, not used) and observer estimates (fed back). (b) Observer error against the encoders over both runs (vertical lines: phases of run I). 9
6 Chisel tip in the strike cycles, from the encoder angles. (a) Descent, press and hold of all eight cycles relative to the planned press point. (b) Mean tip error over the last 2.5 s of the 3-s holds. 9

LIST OF TABLES

I Actuator Parameters Identified by the Auto-Tuning (Run E: Encoder Feedback; Run I: IMU-Only Feedback) 8
II Results of the Machine Experiments 8
III Cross-Validated Joint-Angle Estimation on Real Logs of the Boom (Mean Over Four Train→Test Pairs; Joint Errors in deg, Tip Errors in mm; Lab: Laboratory Implementation) 9
IV Ablation on Identical Sensor Data (One Change per Row) 9